Proceeding of the IEEE
International Conference on Robotics and Biomimetics
Dali, China, December 2019

Design and Analysis of a Flying-crawling Spherical Robot for Multi-mode Movement

Pengfei Lu, Kun Xu* and Xilun Ding
Robotics Institute of School of Mechanical Engineering and Automation, Beihang University
Beijing, China
{lupfi & xk007 & xlding}@buaa.edu.cn

Shuiqing Jiang, Zixin Tang and Yaobing Wang
Beijing Key Laboratory of Intelligent Space Robotic Systems Technology and Applications, Beijing Institute of Spacecraft System Engineering
Beijing, China
ago126@126.com, {zxtang & iamwyb}@163.com

***Abstract* - A novel spherical robot named flying-crawling spherical robot is designed in this paper. It can fly or roll on ground with its single rotor and eight tail fins. When its limbs stretch out it can crawl on the supporting surface. Besides, with its limbs the robot can realize carrying objects, landing on uneven ground and walking on the supporting surface. Dynamic model of the robot in flight mode is established and the motion characteristics are analyzed. A PID control system is designed to enable the robot to achieve stable flight. Trot gait planning of the robot is given and a PID controller is designed for tail fins assistant in crawling mode. Corresponding simulations are carried out and the simulation results verify the proposed methods.**

Index Terms - Spherical UAV, legged robot, structure design, hybrid locomotion system

I. INTRODUCTION

Unmanned aerial vehicle (UAV) is widely used in many fields[1], such as aerial photography, topographic mapping, environmental surveillance, disaster monitoring and electric power routine inspection. In order to enrich the functions of the UAVs and extend their applications, some auxiliary devices such as gripper arm and leg are fixed on it. Small-scale rotorcraft unmanned robotic systems (SRURSs) are a kind of unmanned rotorcraft with manipulating devices and catch much attention of researchers in the world.

The team of Vijar Kumar in University of Pennsylvania is one of the earliest research groups which carried out aerial manipulation. They designed several light-weight, low complexity grippers to allow quadrotors to grasp and perch on branches or beams and pick up and transport payloads[2] and they used a monocular camera to enable their quadrotor to autonomous perch by hanging from cylindrical structures[3]. Ding et al developed a quadrotor with light dual-arm which realized cooperation and climbing[4]. A quadrotor with multi-link arm for assembly tasks was built by Jimenez-Cano A. E. et al in University of Seville[5]. The control method of this aerial robot took into account the motion of the arm and keep the robot stably in the sky. They made another multirotor-based aerial manipulator which consists of eight rotors and a 7-degrees of freedom arm[6]. Besides legs are installed on the UAV. Aerial-Biped robot[7] built in University of Tokyo has quadrotors and two legs. It can float in the air and walk on the ground. Similar as Aerial-Biped robot, Leonardo(LEG ON Aerial Robotic Drone)[8] is also the combination of multi-rotors and dual-leg. It can walk around on lanky legs and can use its thrusters as a failsafe.

Spherical UAV as a special branch has some specific advances. It has a spherical shell which provides shield for the rotors and other equipment. Because of its unique shape the robot can roll along the floor and take off from any orientation. Spherical UAV usually has one single rotor or two coaxial contrary rotating propellers. Two coaxial counter-rotating rotors can compensate their anti-torques, so this structure was used by some researchers. K. Malandrakis et al in Cranfield University designed a spherical UAV to operate mainly in indoor complex environments [9], and a various PD and μ -synthesis control system was designed to stabilize and resistant to external disturbance. A collision-resilient flying robot built in reference [10] has the similar concept and has a protective cage with a three-axis gimbal system. Spherical UAVs studied in references [11,12] also has two contrary rotating rotors. The spherical aircraft with single robot built in Beijing University of Posts and Telecommunications[13] can adjust its orientation by its four flaps and two gravity pendulums and it can roll on the ground. Japanese spherical Drone[14] also uses one rotor, but its details have not been revealed yet. The UNI-Copter[15], a portable spherical UAV has ease of assembly and portability. Though spherical UAVs are safe and reliable for aerial manipulation, most researches on it care less about operating tools.

Based on the above ideas, this paper presents a combination of spherical UAV and quadruped robot, named a flying-crawling spherical robot. It is a hybrid locomotion robot which can realize flying when its limbs fold into its body. The flight function enables it to cross high obstacle or rivers. Besides, it can roll on the ground quickly with its unique shape. When its limbs stretch out, it can crawl on ground with low speed but high stability. It can transform between UAV and quadruped robot, and its limbs can enable the UAV to land on irregular rough terrain. The robot can use its limbs as arms to transport objects to realize aerial manipulation. This paper is organized as follows: section Ⅱ introduces the

* Kun Xu is with the Robotics Institute of School of Mechanical Engineering and Automation, Beihang University (BUAA), Beijing 100191, China (corresponding author to e-mail: xk007@buaa.edu.cn).

978-1-7281-6321-5/19//$31.00 ©2019 IEEE

structure design of the flying-crawling spherical robot and its working modes; section Ⅲ talks about the model analysis and control methods; corresponding simulations of the robot are implemented and results are demonstrated in section IV; in the last, section Ⅴ gives the conclusions.

II. DESIGN OF THE ROBOT

A. *Mechanism and Structure Design of the Robot*

Single rotor is chosen to the spherical robot, and 8 tail fins are used to control the robot body orientation. In order to crawl on ground, four legs each of which has 3 DoFs and is insect configuration are added. The mechanism of the flying-crawling robot is shown as Fig. 1. In total, 21 drivers are needed to control the mechanism to have certain movements.

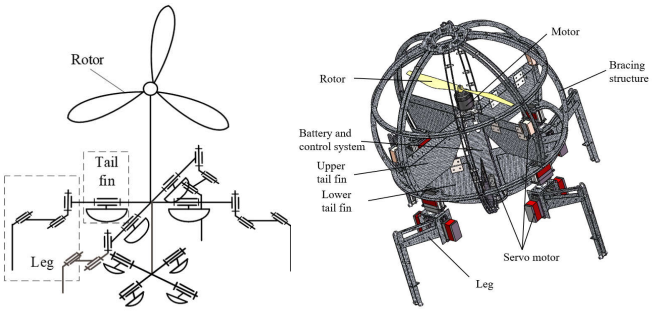

Fig. 1 The mechanism and structure of the robot

3D model of the flying-crawling spherical robot was shown above. Carbon fiber material is chosen to construct the bracing structure of the spherical shell. All equipment of the robot is installed on the bracing structure. Brushless DC motor is installed in the center of the spherical shell. The battery and control system are installed in a rectangular box under the motor. Eight tail fins are installed on the robot and each of them has one active joint which is driven by a servo motor. Four legs are fixed on the bracing structure, even distributed along the rotor axis. Each leg has 3 DoFs and 3 servo motor mounted at the root of the leg. Parallelogram mechanism is used to transmit the motor movement to the shank of the leg.

B. *Working Mode of the Robot*

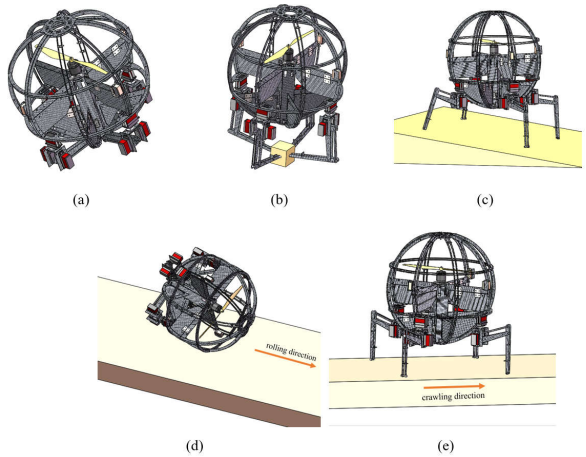

Fig. 3 Working mode of the robot: (a)flying in air; (b) grabbing an object; (c) landing on an inclined plane; (d)rolling on a plane; (e)crawling on a plane.

The spherical robot has five working modes to satisfy different operation needs: flying, grabbing, landing, rolling and crawling, as shown in Fig. 3 above. The four legs of the robot can fold into the spherical shell as shown in Fig. 3a. Under this condition the robot can fly like normal spherical UAV. Because of its spherical body it can also roll on ground (Fig. 3d). When all legs stretch out and contact on the ground the robot can crawl as a quadruped robot (Fig. 3e). When the robot flies its legs also can stretch out. In this condition all legs can be used as arms to grab objects and transport it to another place (Fig. 3b). The legs of the robot do not only enable the robot to walk and manipulate but also supply an adjustable landing platform for the robot. In general condition normal UAVs cannot land on special complex terrain because they may tip over. Because of the discrete support four legs can move their joints to adjust the orientation of the robot body to prevent overturning. The flying-crawling robot can land on rugged terrain with its four legs (Fig. 3c).

III. ANALYSIS AND CONTROL OF THE ROBOT

A. *Flying analysis of the robot*

To simplify the analysis and modeling of the spherical robot in flight, the following assumptions are made：

(1) Compared with the propeller thrust and the lift of tail fins, the drag generated by the fins can be neglected;

(2) The upper four fins and the lower four fins do not interfere with each other in aerodynamics.

(3) The eight fins are completely covered in the propeller airflow, and the airflow velocity below the blade is the same and equal to the average flow speed;

(4) The influence of fuselage frame on airflow is small enough to be neglected;

(5) The deflection angle of each fin is small enough that the angle of attack does not reach the critical point.

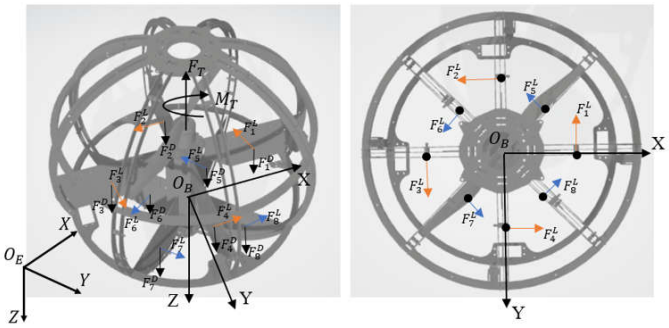

Fig. 4 Model description of the flying-crawling spherical robot

As shown in Fig. 4, a body-fixed frame O_B is created on the robot, whose X axis points to the forward direction of the robot, Z axis goes down along the axis of the motor, and Y axis is determined by the right hand rule. The origin of O_B is located at the center of mass and vector $r_e = [o_x \quad o_y \quad o_z]^T$ denotes its coordinates in world-fixed frame O_E.

A single rotor produces thrust F_T, and torque M_T. The lower part of the rotor has 8 fins uniformly distributed around

the Z axis, and each produces lift F_i^L and drag F_i^D. The upper 4 are used to counteract the motor reverse torque and control the body rotation angle around Z axis (ψ), and the lower 4 are used to control the rotation angle around X axis (ϕ) and Y axis (θ). The two groups of fins are staggered 45 degrees to reduce the interference in aerodynamic. The positive direction of each fin deflection is opposite to the F_i^L produced by itself.

The mass of an aircraft is represented by m, and g denotes gravitational acceleration. The horizontal and vertical distance between the aerodynamic pressure center of the lower fins and the center of mass is set as l_d and h_d, respectively. The horizontal and vertical distance between the aerodynamic pressure center of the upper fins and the center of mass is set as l_u and h_u, respectively.

In the world-fixed frame O_E, the translational dynamic of the robot can be derived as:

$$m\ddot{r}_e = \begin{bmatrix} 0 \\ 0 \\ -g \end{bmatrix} + {}^E R_B \left(\begin{bmatrix} \sum F_x \\ \sum F_y \\ \sum F_z \end{bmatrix} + \begin{bmatrix} 0 \\ 0 \\ -F_T \end{bmatrix} \right) \tag{1}$$

The total force $\sum F_x, \sum F_y, \sum F_z$ is given by

$$\sum F_x = F_4^L - F_2^L + (F_7^L + F_8^L - F_5^L - F_6^L)\cos\frac{\pi}{4} \tag{2}$$

$$\sum F_y = F_3^L - F_1^L + (F_6^L + F_7^L - F_5^L - F_8^L)\cos\frac{\pi}{4} \tag{3}$$

$$\sum F_z = F_1^D + F_2^D + F_3^D + F_4^D + F_5^D + F_6^D + F_7^D + F_8^D \tag{4}$$

In the body-fixed frame O_B, the rotational dynamic of the robot can be derived as:

$$I\dot{\omega} = \begin{bmatrix} \sum M_x \\ \sum M_y \\ \sum M_z \end{bmatrix} + \begin{bmatrix} 0 \\ 0 \\ M_T \end{bmatrix} - \omega \times I\omega \tag{5}$$

where I denotes the inertia of the robot and $\omega = [p \quad q \quad r]^T$ denotes the angular velocity in frame O_B.

The total moment produced by tail fins $\sum M_x, \sum M_y, \sum M_Z$ is given by

$$\sum M_x = (F_3^L - F_1^L)h_u + (F_5^L + F_8^L - F_6^L - F_7^L)h_d \cos\frac{\pi}{4} + (F_4^D - F_2^D)l_u + (F_7^D + F_8^D - F_5^D - F_6^D)l_d \cos\frac{\pi}{4} \tag{6}$$

$$\sum M_y = (F_2^L - F_4^L)h_u + (F_7^L + F_8^L - F_5^L - F_6^L)h_d \cos\frac{\pi}{4} + (F_3^D - F_1^D)l_u + (F_6^D + F_7^D - F_5^D - F_8^D)l_d \cos\frac{\pi}{4} \tag{7}$$

$$\sum M_z = -(F_1^L + F_2^L + F_3^L + F_4^L)l_u - (F_5^L + F_6^L + F_7^L + F_8^L)l_d \tag{8}$$

Using ${}^E R_B$ as rotation matrix from body-fixed frame O_B to world-fixed frame O_E. ϕ, θ, ψ denotes the angles of rotations around x, y, z axis respectively and c, s denotes cos and sin respectively. ${}^E R_B$ can be written as

$${}^E R_B = \begin{bmatrix} c_\psi c_\theta & c_\psi s_\phi s_\theta - c_\theta s_\psi & s_\phi s_\psi + c_\phi c_\psi s_\theta \\ c_\theta s_\psi & c_\theta c_\psi + s_\psi s_\phi s_\theta & c_\phi s_\psi s_\theta - c_\psi s_\phi \\ -s_\theta & c_\theta s_\phi & c_\phi c_\theta \end{bmatrix} \tag{9}$$

As the spherical aircraft is usually in a small angle flight, the body angle ϕ, θ and angular velocity $\dot{\phi}, \dot{\theta}$ is around zero. So the translational dynamics (1) can be written as

$$m\ddot{v}_B - \begin{bmatrix} 1 & \psi & -\theta \\ -\psi & 1 & \phi \\ \theta & -\phi & 1 \end{bmatrix} \begin{bmatrix} 0 \\ 0 \\ mg \end{bmatrix} = \begin{bmatrix} \sum F_x \\ \sum F_y \\ \sum F_z \end{bmatrix} + \begin{bmatrix} 0 \\ 0 \\ -F_T \end{bmatrix} \tag{10}$$

Assuming that drag F_i^D is negligible compared to lift F_i^L and thrust F_T. It can be derived from (5) and (10) as

$$\begin{cases} m\dot{v}_x + mg\theta = \dfrac{\sum M_y}{h} \\ m\dot{v}_z - mg = -F_T \\ m\dot{v}_y - mg\phi = -\dfrac{\sum M_x}{h} \end{cases} \tag{11}$$

$$\begin{cases} I_{xx}\dot{p} + qr(I_{zz} - I_{yy}) = \sum M_x \\ I_{yy}\dot{q} + pr(I_{xx} - I_{zz}) = \sum M_y \\ I_{zz}\dot{r} = u_\psi + k_M F_T \end{cases} \tag{12}$$

where k_M denotes the proportionality coefficient between M_T and F_T.

The motor thrust is modelled as

$$F_T = K_f u_T \tag{13}$$

where u_T is the PWM input of the motor and K_f denotes the maximum thrust produced by the motor.

The lift equation is

$$L = \frac{1}{2} C_l \rho v^2 A \tag{14}$$

where C_l is lift coefficient, ρ is air density, v is air velocity, and A is fins area. Using A_{prop} as the area of propeller, v is derived by momentum conservation as

$$v = \sqrt{\frac{F_T}{2\rho A_{prop}}} \tag{15}$$

When the fins deflect at a small angle, the lift coefficient C_l is approximately proportional to the rotation angle. So the lift F_i^L produced by tail fins can be derived as

$$F_i^L = \frac{F_T C_{lift} A \alpha_i}{2A_{prop}} \tag{16}$$

Where α_i denotes angle of tail fins and C_{lift} is the proportionality coefficient between C_l and α_i. Assuming $K_L^u = \frac{C_{lift} A_u}{2A_{prop}}$ and $K_L^d = \frac{C_{lift} A_d}{2A_{prop}}$ where A_u and A_d denote the area of upper fins and lower fins respectively, the lift generated by tail fins can be derived as

$$F_i^L = K_L^u K_f u_T \alpha_i \ (\mathrm{i}=1、2、3、4) \tag{17}$$

$$F_i^L = K_L^d K_f u_T \alpha_i \ (\mathrm{i}=5、6、7、8) \tag{18}$$

The moment generated by motor is

$$M_T = K_T u_T \tag{19}$$

where K_T denotes the maximum moment produced by the motor. The resultant force and moment can be derived by substituting F_i^L in (2-4) and (7-9) with (17-18). When the 4 upper fins have the same deflection angle, (11) and (12) can be rewritten as

$$\begin{cases} m\dot{v}_x + mg\theta = \dfrac{\sqrt{2}}{2} \mathrm{K}_L^d \mathrm{K}_f u_T (\alpha_7 + \alpha_8 - \alpha_5 - \alpha_6) \\ m\dot{v}_z - mg = -\mathrm{K}_f u_T \\ m\dot{v}_y - mg\phi = \dfrac{\sqrt{2}}{2} \mathrm{K}_L^d \mathrm{K}_f u_T (\alpha_6 + \alpha_7 - \alpha_5 - \alpha_8) \end{cases} \tag{20}$$

$$\begin{cases} I_{xx}\dot{p} + qr(I_{zz} - I_{yy}) = \dfrac{\sqrt{2}}{2} K_L^d K_f u_T h_d (\alpha_5 + \alpha_8 - \alpha_6 - \alpha_7) \\ I_{yy}\dot{q} + pr(I_{xx} - I_{zz}) = \dfrac{\sqrt{2}}{2} K_L^d K_f u_T h_d (\alpha_7 + \alpha_8 - \alpha_5 - \alpha_6) \\ I_{zz}\dot{r} = -K_L^u K_f u_T l_u (\alpha_1 + \alpha_2 + \alpha_3 + \alpha_4) - \\ K_L^u K_f u_T l_d (\alpha_5 + \alpha_6 + \alpha_7 + \alpha_8) + K_T u_T \end{cases} \tag{21}$$

B. *Flight control system*

In order to achieve flight stability, a PID control system is designed as shown in Fig. 5.

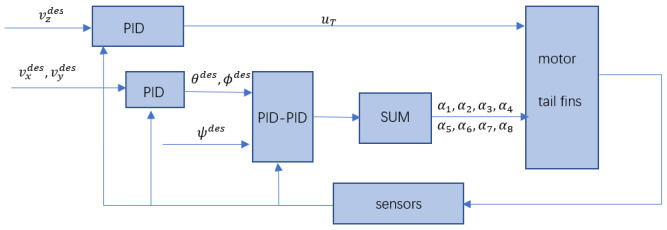

Fig. 5 Flight control system of the robot

The control system has 4 inputs, $v_x^{des}, v_y^{des}, v_z^{des}, \psi^{des}$ which denote the expected velocity in x, y, z axis and the expected rotational angle around z axis respectively. The outputs of outer PID are $u_T, \theta^{des}, \phi^{des}$,which denote the expected motor speed, angular velocity around y and x axis respectively. θ^{des}, ϕ^{des}, combined with ψ^{des}, are inputs of inner PID which outputs u_1, u_2, u_3. Sensors get the attitude of the robot as feedback information, and the SUM module translates u_1, u_2, u_3 to α_i as

$$\begin{aligned} &\alpha_1 = \alpha_2 = \alpha_3 = \alpha_4 = -u_3 \\ &\alpha_5 = -u_1 + u_2 \\ &\alpha_6 = u_1 + u_2 \\ &\alpha_7 = u_1 - u_2 \\ &\alpha_8 = -u_1 - u_2 \end{aligned} \tag{22}$$

C. *Trot gait planning of the robot*

The quadruped robot can walk in static gait or in dynamic walking gait. When the robot walks in complex terrain, static gait can improve stability and reduce the probability of dumping. But the traveling velocity is slower. In order to get a faster moving speed, the robot should adopt the dynamic walking gait. Dynamic walking gait is a kind of progressive state in which the robot relies on dynamic balance and stability while advancing. It relies on gravity, inertia force, centrifugal force and so on to keep the robot in a sustainable and stable state.

The gait of quadruped robot includes Trot, Pace, Bound, Gallop and so on. Trot gait is a diagonal gait, in which 2 legs of the robot on the diagonal line are lifted and landed at the same time as it moves forward. Pace is a gait in which two legs on one side of the robot are lifted and dropped at the same time. Bound is a jumping gait in which the front two legs and the back two legs of the robot land alternately. Gallop is the running gait of a quadruped robot with four legs in different phases.

The center of gravity (COG) trajectory planning method proposed by Pongas D, Mistry M and Schaal S [16] is used to plan the motion trajectory of the robot in static gait. But it won't be given a detailed description here. In dynamic walking gait, bound and gallop advance fastest, but they have high requirements on robot structure, driver and algorithm which makes it hard to achieve. Pace gait is prone to rollover and difficult to control. Trot gait is symmetrical and its control is relatively simple. Besides, the cog projection on ground is near to the diagonal line formed by two support legs. This characteristic will bring convenience to attitude control by tail fins in next subsection. So, trot gait is adopted when the robot moves fast.

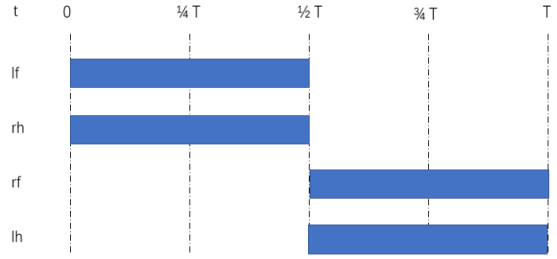

Fig. 6 Sequence diagram of trot gait: Dark areas indicate that this leg is in the supporting phase, and blank areas indicate that this leg is in the swing phase. t denotes time and T denotes time of a motion cycle. lf, rh, rf and lh denote the left-front, right-hind, right-hind and left-hind foot respectively.

In order to reduce the impact of bumper when legs fall to the ground, cycloidal trajectory is used in swing phase trajectory planning.

D. *Flying-crawling control of the robot*

The trot gait plan above is regardless of dynamic model of the robot and complex terrain. It will be easy to roll over when walk on terrain or be disturbed by external force. So, the flying-crawling control method was proposed to improve its crawling performance.

In flying-crawling mode, the propeller applies fixed thrust to body to reduce its gravity, which reduces the impact of bumper when legs fall to ground. The tail fins will deflect to maintain the attitude stability. Unlike flight mode, the upper 4 fins will be used to control pitch and roll angle because they have a longer arm of force and also larger area, and the lower 4 fins will be used to control yaw angle. A PID controller was used to control 8 fins as shown in (23).

$$\begin{aligned} u_\phi &= k_{p1}(\phi_{des}-\phi)+k_{i1}\int(\phi_{des}-\phi)dt+k_{d1}p \\ u_\theta &= k_{p2}(\theta_{des}-\theta)+k_{i2}\int(\theta_{des}-\theta)dt+k_{d2}q \\ u_\psi &= k_{p3}(\psi_{des}-\psi)+k_{i3}\int(\psi_{des}-\psi)dt+k_{d3}r \end{aligned} \tag{23}$$

The $\phi_{des},\theta_{des},\psi_{des}$ denotes desired roll, pitch, yaw angle respectively, and $k_{pj},k_{dj},k_{ij}(j=1,2,3)$ denotes coefficient of PID controller respectively.

IV. Simulations of the Robot

A. *Flying simulation by gazebo*

To verify the availability of the flight control system in Fig. 5, a robot model was built in gazebo, an independent open source simulation platform. As the robot can move in diffident ways, gazebo was suitable. All simulations were done in gazebo by adding force directly to tail fins or propeller of robot model.

The simulation parameters are set as shown in Table I. A simulated velocity step-response in z-axis and attitude response for roll, pitch and yaw angle is presented in Fig. 7.

TABLE I
Flying Simulation Parameters

Parameter	value	Units
m	2.2	kg
I_{xx}	0.1092	$kg\cdot m^2$
I_{yy}	0.11	$kg\cdot m^2$
I_{zz}	0.033	$kg\cdot m^2$
I_{xy},I_{yz},I_{zx}	0	$kg\cdot m^2$
h_d	0.106	m
l_u	0.122	m
l_d	0.083	m
K_f	41.2	N
K_T	0.5	N
K_l^u	0.0708	——
K_l^d	0.0549	——

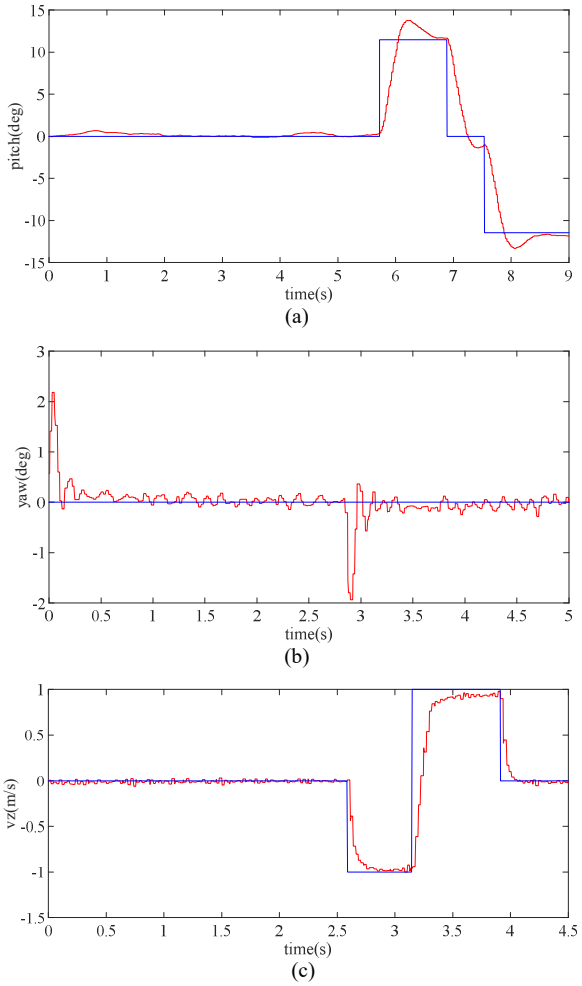

Fig. 7 Simulation results for step response test

Fig. 7 shows the flight tests in simulation. Red line denotes real state of the robot and blue line denotes command input. The robot showed stable flight performance. The simulation started at 0 seconds and the robot started to take off. Then yaw angle changed to around 2 degrees quickly (Fig .7b) because of counter torture caused by motor start. But the yaw angle returned to 0 in around 0.3s and then slightly fluctuated up and down near zero. The yaw angle changed to -2 degrees at around 2.8 seconds because manual input was added to stop rising. After the robot takeoff and became steady in height, a step input of pitch angle was added at 5.5 seconds to test its step response (Fig. 7a). The pitch angle reached 10 degrees in around 0.5 seconds with little oscillation. A same step input was added to roll angle and the robot showed similar response because of symmetry in structure. In another flight simulation, a step input was added to VZ (velocity in z-axis). The robot reached 1m/s in around 0.3 seconds and then became steady again (Fig. 7c).

B. *Crawling simulation by gazebo*

In order to verify the crawling control in section III, model of the robot and simulation environment was built in gazebo. Fig. 8 shows two crawling cycle when the robot moved forward.

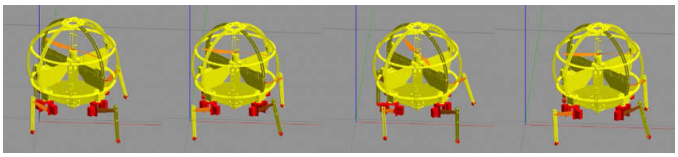

Fig. 8 Simulation environment in gazebo

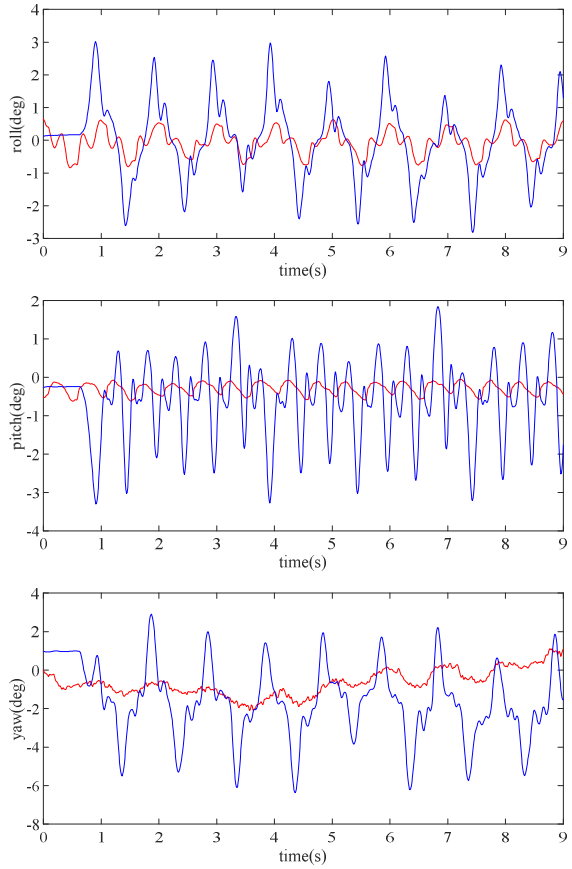

Fig. 9 Simulation results for crawling

Fig. 9 shows the attitude of the robot when the robot crawl forward. The advance velocity was 0.15m/s and T was set to 1 seconds. The blue line shows the attitude change during crawling without attitude control by tail fins. The roll angle, ϕ, maintained within 6 degrees. The pitch angle, θ, maintained within 5 degrees. And the yaw angle Ψ was kept within 8 degrees. The red line shows the attitude change when propeller and tail fins were used to control attitude. In the flying-crawling mode, the robot showed stable performance. The roll angle was kept in 1.5 degrees, the pitch angle was kept in 0.5 degrees and the yaw angle was kept in 2 degrees.

V. Conclusion

This paper presented a novel concept named flying-crawling spherical robot which combines spherical UAV and quadruped robot. It has 4 movement modes, flying, rolling, crawling and flying-crawling. When the robot needs to cross the river, mountain and other complex terrain, it can fly quickly. With the rolling function, it can also move quickly on flat ground. In crawling mode, the robot can move in a small range to manipulate and the flying-crawling mode provide a more stable and safe movement.

The flying mode was analyzed and a PID control system was designed to enable the robot to fly stably. Gait planning of the robot was given. Corresponding simulations were carried out and some results are demonstrated in this paper. The results of simulation verified the flying and crawling move ability of the robot. But the conversion process between the 4 modes was not researched in detail, and energy consumption of 4 modes was not given quantificationally. This should be the future work.

Acknowledgement

This research was supported by National Key R&D Program of China (2017YFB1300400) and National Natural Science Foundation of China (No.51775011 & No.91748201).

References

[1] Xilun DING, Pin GUO, Kun XU, Yushu YU. A review of aerial manipulation of small-scale rotorcraft unmanned robotic systems. Chinese Journal of Aeronautics 2019; 32(1):200-214.

[2] Mellinger, D., Lindsey Q. et al., Design, modeling, estimation and control for aerial grasping and manipulation, in 2011 IEEE/RSJ International Conference on Intelligent Robots and Systems. 2011. p. 2668 - 2673.

[3] Thomas J, Loianno G, Daniilidis K, et al. Visual Servoing of Quadrotors for Perching by Hanging From Cylindrical Objects[J]. Robotics & Automation Letters IEEE. 2016.

[4] Ding X, Yu Y, Zhu J J. Trajectory linearization tracking control for dynamics of a multi-propeller and multifunction aerial robot - MMAR[J]. IEEE International Conference on Robotics & Aut... 2011.

[5] Jimenez-Cano A E, Martin J, Heredia G, et al. Control of an aerial robot with multi-link arm for assembly tasks[J]. 2013.

[6] Heredia G, Jimenez-Cano A E, Sanchez I, et al. Control of a multirotor outdoor aerial manipulator[J]. 2014.

[7] https://www.cnbeta.com/articles/science/757117.htm?agt=589

[8] This Birdlike Robot Uses Thrusters to Float on Two Legs, https://www.wired.com/story/this-bird-like-robot-uses-thrusters-to-float-on-two-legs/. 2019

[9] Malandrakis K , Dixon R , Savvaris A , et al. Design and Development of a Novel Spherical UAV[J]. IFAC PapersOnLine, 2016, 49(17):320-325.

[10] A. Briod, P. M. Kornatowski, et al. A collision resilient flying robot[J]. Journal of Field Robotics, 31(4) (2014) 496-509.

[11] Matassini T , Shin H S , Tsourdos A , et al. Adaptive Control with Neural Networks-based Disturbance Observer for a Spherical UAV[J]. IFAC PapersOnLine, 2016, 49(17):308-313.

[12] Gui H , Senchun C , Lingguo C , et al. Attitude control of spherical unmanned aerial vehicle based on Active Disturbance Rejection Control[C]// Control Conference. IEEE, 2015.

[13] Peng Li. Design and flight characteristics research of a spherical aircraft[D]. Beijing University of Posts and Telecommunications, 2013.

[14] New Atlas,Japanses Defense Ministry shows world's first spherical flying machine, http://www.newatlas.com/Japanese-spherical-flying-machine/20286(2011)

[15] Jae-Sung M , Choonghyun K , Youngil Y , et al. UNI-Copter: A portable single-rotor-powered spherical unmanned aerial vehicle (UAV) with an easy-to-assemble and flexible structure[J]. Journal of Mechanical Science and Technology, 2018, 32(5):2289-2298.

[16] Pongas D , Mistry M , Schaal S . A robust quadruped walking gait for traversing rough terrain[C]// IEEE International Conference on Robotics & Automation. 2007.